HAPP: a Haptic Portable Pad for Hand Disease Manual Treatment

Mihai Dragusanu[1*], Danilo Troisi[1,2*], Alberto Villani[1], Domenico Prattichizzo,[1,3] and Monica Malvezzi[1]

***Abstract*— Nowadays, especially with the Covid-19 pandemic, researchers are focusing their attention on the remote delivery of devices designed for rehabilitation purposes, allowing people to recover without the physical presence of a doctor. Manual therapy is a physical treatment that is used by therapists for the treatment of musculoskeletal pain and/or disabilities. The aim of this work is to present HAPP, a new haptic portable device, designed to help patients suffering of different patholohgies, as for instance the Complex Regional Pain Syndrome type-I disease, and more in general to investigate the effects of manual therapy for diseases of the carpus and metacarpus, by mimicking traditional mechanical and rhythmic stimuli characteristics of manual treatments. Its structure consists of a plate oriented by revolute-prismatic-spherical joints, with a rack-pinion mechanism that actuates the end-effector, stimulating the user's hand palm. We provide details about the device, such as the mechanical design, the mathematical model and a graphical user interface. Preliminary studies in order to evaluate the device force exerted at the user's palm were carried out.**

I. Introduction

Hands are the primary tactile interfaces that allow humans to interact, experience, move and/or shape the matter around them. However, hands are often affected by injuries, fractures, sprain, tissue pathologies, diseases that develop chronic pains or syndromes, as for instance the stroke, diabetes or the complex regional pain syndrome type-I (CRPS-I). In particular, the CRPS-I is a chronic painful syndrome consisting of several alterations of perceived sensation as allodynia (pains for normally elicit pain stimulus), hyperalgesia (abnormal increase of sensitivity to pain), edema (the build-up of fluid in the body's tissue), vasomotor/sudomotor deregulation and tissue trophism modification. These symptoms spread from distal regions of the affected hand/arm to the opposite limb [1], [2], [3], [4]. Traditional clinical therapy for CRPS-I consists in patient education to pain management, desensitization therapy, manual therapy (MT) and progressive exercises to improve the strength and flexibility of the affected hand [5], [6], [7]. Manual therapy (i.e., joint mobilizations, rhythmic stimulation and force applications) is a common treatment for many other painful hand conditions and an adjunct treatment musculoskeletal conditions [8]. Regarding the effects on CRPS-I, the manual therapy allows to alleviate pains and improve hand functionality, according with [9], [10]. The literature about CRPS treatment with MT is still poor of information about pathophysiology of this syndrome. According with preliminary *in-vivo* investigation, presented in [2], [11], [12], this therapy has analgesic effects in mice, allowing the activation of inhibitory of neuroreceptors (adenosine, opioid, and cannabinoid). In [13], an *in-vitro* study assessed that MT activates enzymatic anti-oxidative system, reducing the oxidative stress, which is responsible of an inflammatory event cascade, and, consequently, alleviating the pain.

Fig. 1: HAPP prototype during preliminary investigation.

Haptic technologies are widely used in preclinical investigation and then in therapy. For example, it has been shown in [14] that the use of haptic technologies can simplify the transition of children with autism spectrum disorder during occupational therapies. In [15], the authors corroborated the feasibility hypothesis of a mechanical therapy for cardiovascular autonomic control in Parkinson's disease.

Research in the field of haptics has often provided clinical tools for the rehabilitation and specific treatment for joint, ligament and skin issues of hands. As reported in [16] by Choukou et al., different haptic technologies combined with robots ([17], [18], [19]), virtual reality (VR) environments and games ([20], [21], [22]) or both ([23], [24]) have been involved for the rehabilitation of the paretic upper limb of stroke patients. Bouri et al. in [25] presented an innovative haptic device designed specifically for the rehabilitation of hemiplegic children, which activates their hand joints, similarly to MT. In [26] and [27], the authors investigated about new haptic technologies to overall problems with handwriting or drawing due to graphomotor issues; they designed technologies and the protocol for the assessment and therapy for eye-hand coordination. Ferre et al., as reported in [28], realized a haptic framework that captures and mimics manual therapy techniques using a multifinger device.

In this paper, leveraging our expertise in hand stimulation by haptic devices [29], [30] and robotic systems for reha-

[1]are with the Department of Information Engineering and Mathematics, University of Siena, Siena, Italy {dragusanu, villani, ndaurizio, prattichizzo, malvezzi}@diism.unisi.it.

[2]are with the Department of Information Engineering, University of Pisa, Pisa, Italy {danilo.troisi@phd.unipi.it}

[3]are with the Department of Advanced Robotics, Istituto Italiano di Tecnologia, Genova, Italy. {domenico.prattichizzo}@iit.it

*Equally contributed to this work.

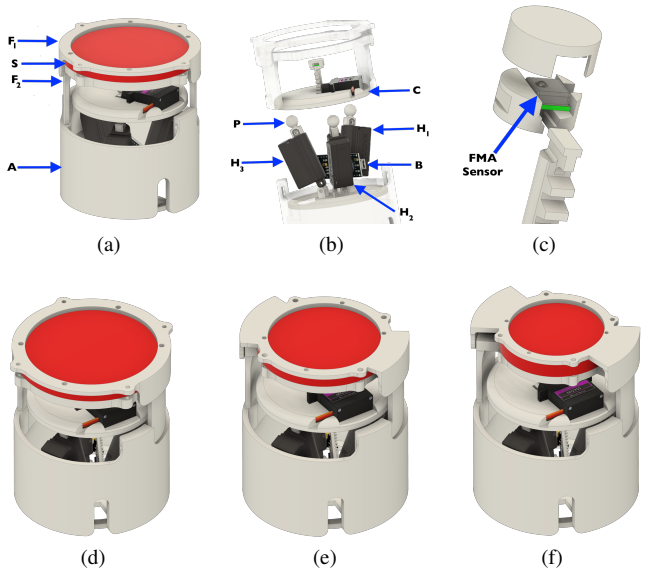

Fig. 2: HAPP main features. (a) HAPP external CAD model. (b) HAPP internal CAD model. (c) CAD model for the FMA sensor housing. (d),(e),(f) CAD model of the top part with different sizes, i.e. large (a), medium (b) and samll (c).

bilitation [31], [32], [33], we present HAPP (see Fig. 1), a haptic device for preclinical investigation on correlation between CRPS-I symptoms reduction and MT, and also for clinical treatment of CRPS-I and other diseases of carpus and metacarpus, by mimicking traditional mechanical and rhythmic stimulations proper of manual treatments. The haptic device design presented in Sec. II consists in parallel kinematic structure with 3-Degrees of Freedom (DoFs) that planarly moves and orients its interchangeable end-effector under the hand palm of the patient and provide locally a different mechanical stimulation according with needs and interests of the researcher; in the current version of the prototype, we designed an end-effector that exerts controlled force, which stimulates predefined contact area of the hand palm. A silicone rubber pad is inserted between patient palm and end-effector. This material was chosen to allow the sterilization of the device; however, since the presence of silicone alters the effects of the forces provided to patient, theoretical study and tests for actual device force are reported in Sec. IV. Conclusion and future studies are reported in Sec. VI.

II. Device Description

In this section, we will detail the design and the hardware components used for HAPP. The CAD model of the device is shown in Fig. 2: all its components were printed in Acrylonitrile Butadiene Styrene (ABS) using FDM (Fused Deposition Modeling) technique. It is made up of two main parts: a fixed one, called *bottom part* and an interchangeable one, called *top part*. The *bottom part* consists of the housing for the electronic part, the actuation module, and a circular plate that contains the end effector of the device, respectively **B**, $\mathbf{H}_i$ and **C** in Fig. 2b. The *top part* is in contact with the user's hand palm and it is designed in such a way to be easily assembled with the support base (**A** in Fig. 2a) by making a twisting motion.

The device allows the interchangeability of different structures that support the human hand. Indeed, in order to adapt the device to the needs of users with different anthropometric dimension of the hand, the *top part* structure has been made in different sizes, i.e. small, medium, and large (see Fig. 2d,2e,2f). Part **C** of the device constitute the end-effector of the device. This circular plate contains the housing for a servomotor, which is used to actuate the rack-pinion mechanism. The servomotor used is a Kuman MG90S (Kuman Trade Shenzhen Co., Ltd., US) with a stall torque of 25 Ncm at 6V. The shaft allows HAPP to exert the desired force on defined areas of the device that lie on the *top part*. With the aim to allow different types of stimuli at user's palm the shaft head has been made interchangeable. In Fig. 2c the CAD model of the force sensor embodiment is shown. The sensor used is the FMA MicroForce Sensor FMAMSDXX025WCSC3 (Honeywell, North Carolina), a piezoresistive based force sensor that provides a digital output proportional to the force applied on it. The FMA version with a force range of 25N and an accuracy of 0.5N was chosen and it is interfaced using SPI protocol. It has a maximum digital clock frequency of 800kHz and it is powered with an operating voltage of 3.3V. Furthermore, part **C** of the device plays a fundamental role in the orientation of the end-effector, since its lower part contains the spherical-shaped housings, which constitute the spherical joints between the actuation module $\mathbf{H}_i$ and the part **C**. These spherical housings are arranged in a particular shape, i.e. they are Y-shaped and consequently also the actuators are arranged in the same way. The actuators used are the Actuonix PQ12-P, which have a maximum stroke of 20 mm and exert a maximum force of 45N. The characteristics of these linear actuators are summarized in Tab. I. Three actuators are used to move and orient the plate **C**, which is connected to them through a rigid-spherical link, indicated with **P**. Furthermore, the linear actuators are not positioned vertically with respect to the plate but are inclined by 45° each with the aim to ensure device stability, structural robustness and compactness. The device configuration is controlled with Arduino Nano 3.0.

In order to avoid direct contact of the shaft with the user's palm, the *top part* of the device is made up of two parts, i.e. **F1** and **F2**. They allow the insertion of a material **S**, which is soft to the touch and capable of being sterilized whenever the device is used. **F1** is connected to the *bottom part* of the device, while **F2** is fixed to **F1**. The material inserted between these two parts is made of silicone rubber. The cylindrical elastic pad is realized by molding and curing for four hours bi-component silicone rubber Eco-flex 00-30 (Smooth-On, inc. US) with platinum catalyst. The platinum catalyst allows the containment of the hardness of the silicone in a range of $[0-30]$ on the Shore A scale (ASTM D-412). The mold is fabricated by 3D-

TABLE I: Main characteristics of the PQ12-P linear actuator

Technical Features	
Mass	15 g
Max. Force (lifted)	45 N
Stroke	20 mm
Feedback Potentiometer	5 kΩ
Stall Current	550 mA @ 6V
Max Duty Cycle	20 %
Max Speed (no load)	15 mm/s

printing in ABS and coated with a mold releaser, the Easy Release 200 (Mann Release Technologies, inc. US), to ease extract the pad after the cure phase. The chemical properties of this silicone rubber, as we said, allow the sterilization of the pad that is in contact with the patient's palm both with chemical agent 70 % ethanol (CH3CH2OH) cleaning reagent and autoclaving, since the silicone rubber hold its elastic proprieties up to 230°C, while the normal autoclaving temperature is about 180°C.

III. Mathematical model

A. Configuration analysis

From the kinematics point of view, HAPP is a 3-RPS (Revolute-Prismatic-Spherical), 3-DoF (Degrees of Freedom) parallel mechanism. Let us indicate with B_i, $i = 1, 2, 3$ the centers of the spherical joints on the *end effector* $\mathbf{C}$, with O_1 the center of the circle passing through them, and with b its radius. Let us also indicate with $S_1 = \langle O_1, x_1, y_1, z_1 \rangle$ a reference frame in which the x_1 axis is parallel to $\overrightarrow{O_1 B_1}$, z_1 is orthogonal to the plane defined by the B_i points, and y_1 is consequently defined. We assume that B_i points form an equilateral triangle, the coordinates of each vertex B_i, expressed in the S_1 reference frame are collected in the three-dimensional vectors $\mathbf{b}_i^1 = [b_{ix}^1, b_{iy}^1, b_{iz}^1]^{\mathrm{T}}$.

Each leg is composed of two links: the first is connected to the fixed base trough a revolute joint, the second one is connected to the end effector through a spherical joint. The links are connected to each other through a prismatic joint. Let us indicate with $\mathbf{u}_i$ the unit vector identifying, for each leg, the direction of the revolute joint axes. We can then define the plane π_i passing through B_i and perpendicular to $\mathbf{u}_i$. The revolute joint axes intersect this plane in A_i points

On the *bottom part*, we define O_0 as the center of the circle passing through A_i, and with a its radius. Let $S_0 = \langle O_0, x, y, z \rangle$ be a reference frame on the *bottom part*, with origin in O_0, x axis parallel to the $\overrightarrow{O_0 A_1}$ vector, z axis orthogonal to the plane defined by A_i points, and y consequently defined. Also in this case we assume that A_i points define a equilateral triangle.

The end effector will move w.r.t. the *bottom part* according to the displacement imposed by the linear actuators and to the kinematic constraints imposed by the mechanical structure. In particular the motion of each leg is plane, i.e. B_i points move on the planes previously introduced π_i.

Indicating with i_*, j_*, k_*, $* = x, y, z$, the unit vectors components corresponding to the axes x_1, y_1, and z_1, respectively, expressed w.r.t. S_0, we can define the corresponding rotation matrix $\mathbf{R}$ between S_1 and S_0.

The coordinates of B_i w.r.t. S_0, collected in the three dimensional-vectors $\mathbf{b}_i = [b_{i,x}, b_{i,y}, b_{i,z}]^{\mathrm{T}}$, can be evaluated as

$$\mathbf{b}_i = \mathbf{p} + \mathbf{R}\mathbf{b}_i^1, \tag{1}$$

where $\mathbf{p} = [p_1, p_2, p_3]^{\mathrm{T}}$ is the three dimensional vector containing the coordinates of O_1 w.r.t. S_0.

Since B_i move on the three fixed planes π_i, the following constraint equations hold

$$b_{1,y} = 0, \quad b_{2,x} = \frac{1}{\sqrt{3}} b_{2,y}, \quad b_{3,x} = -\frac{1}{\sqrt{3}} b_{3,y}. \tag{2}$$

Eq. (2) introduces three constraints that limit the generic six–dimensional motion of the mobile platform. In particular, since three independent costraints have been introduced, the mobile platform has three DoF.

The position and orientation of the end effector can be defined by the position and orientation of O_1 w.r.t. S_0, described through its coordinates $\mathbf{p} = [p_x, p_y, p_z]^{\mathrm{T}}$ and Roll(α)–Pitch(β)–Yaw(ϕ) angles $\boldsymbol{\varphi} = [\alpha, \beta, \phi]^{\mathrm{T}}$, respectively. Since the platform has 3 DoF, we can select three of these six variables and evaluate the remaining ones. A convenient choice for the *independent* variables includes the displacement in the z direction, p_z, and the roll (α) and pitch (β) angles. Let us collect those variables in the vector $\boldsymbol{\xi} = [p_z, \alpha, \beta]^{\mathrm{T}}$. Recalling the rotation matrix expression as a function of RPY angles, and the constraints in eq. (2), we can evaluate the other variables as

$$\phi = \arctan\left(\frac{\sin\beta \sin\alpha}{\cos\beta + \cos\alpha}\right), \tag{3}$$

$$p_x = \frac{b}{2}\left(\cos\phi\cos\beta - \sin\phi\sin\beta\sin\alpha - \cos\phi\cos\alpha\right), \tag{4}$$

$$p_y = -b\sin\phi\cos\beta. \tag{5}$$

To complete the preliminary analysis of the mechanism, let us analyse the position of the pin on the mobile platform, represented by point R. Its coordinates in S_1 frame are:

$$\mathbf{r}^1 = [0, 0, h]^{\mathrm{T}}, \tag{6}$$

using the above mentioned relationships, it is possible to evaluate its coordinates with respect to S_0 frame. Finally, using the relationships in eq. (3),(4), and (5) it's possible to express pin position as a function of the independent variables, i.e. $\mathbf{r}(\boldsymbol{\xi})$.

B. Inverse kinematics

In the inverse kinematics problem, the independent variables $\boldsymbol{\xi} = [p_z, \alpha, \beta]^{\mathrm{T}}$ are defined, and we want to evaluate the corresponding displacements $\mathbf{q} = [q_1, q_2, q_3]^{\mathrm{T}}$ of the linear actuators. For a given $\boldsymbol{\xi}$, eq. (3), (4), and (5) allow to define the vector $\mathbf{p}$ and the rotation matrix $\mathbf{R}$, completing the representation of the mobile platform configuration. Then, from eq. (1), it is possible to evaluate the coordinates of B_i w.r.t. S_0. The actuator displacements q_i can be then evaluated as

$$q_i = s_i - l_0, \tag{7}$$

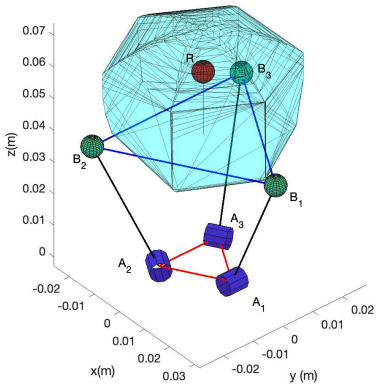

Fig. 3: HAPP kinematic scheme and and workspace evaluation (cyan solid). The workspace is represented as the set of possible positions that R point can assume, considering actuators' strokes and device kinematic constraints.

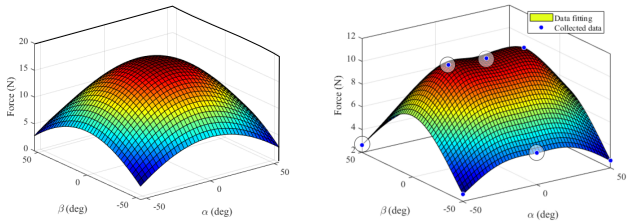

(a) (b)

Fig. 4: In (a), the theoretical net force distribution through HAPP silicon pad depending on EE orientation angles α and β, in (b) the experimentally estimated net forces reconstructed for symmetry and interpolation by means of repeated force measures in four notable points (circled blue dots).

where $s_i = |\mathbf{b}_i - \mathbf{a}_i|$ and l_0 is the actuator length in its reference configuration.

The above described relationships have been used to evaluate the device workspace, i.e. the set of positions that point R can reach, given device kinematic structure and actuator stroke. The obtained workspace, calculated by means of a Matlab script, is shown in Fig. 3.

To evaluate the force executable by HAPP on patient palm, a theoretical study and an experimental investigation were carried out. The net theoretical force $\boldsymbol{f}_n$ on the palm depends on the end-effector orientation angles α and β respect normal

TABLE II: Joint extensions and relative orientation angles of end-effector to reach the four selected points for maximum net force distribution reconstruction.

Point	$p_{H1}(mm)$	$p_{H2}(mm)$	$p_{H3}(mm)$	α (deg)	β (deg)
1	20.0	0.0	20.0	-50.0	50.0
2	20.0	0.0	0.0	0.0	50.0
3	0.0	10.0	20.0	-25.6	25.6
4	20.0	20.0	20.0	0.0	0.0

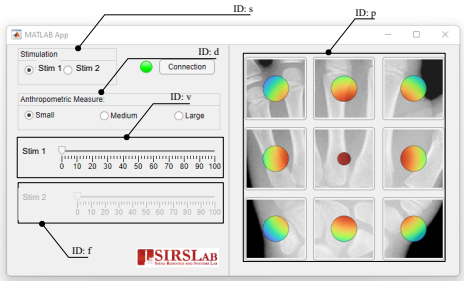

Fig. 5: Graphical User Interface for HAPP.

vector of the silicone rubber plane (in this evaluation, yaw angle ϕ has been neglected, since its value is limited in all the considered configurations).

$$\mathbf{f}_n(t) = |\mathbf{f}_b| \cos(\alpha) \cos(\beta), \tag{8}$$

where $|\boldsymbol{f}_b|$ is modulus of the normal force in *bottom part* reference frame evaluated as effect of the end-effector indentation in silicone rubber pad:

$$|\mathbf{f}_b| = \frac{l_2 - l_1}{l_1} \pi \rho_{EE}^2 E,$$

with $\frac{l_2 - l_1}{l_1}$ is the material deformation (l_1 and l_2 are the thins of pad before and after indentation), ρ_{EE} is the radius of the end-effector contact area, and E is the approximated Young modulus of neo-Hookean material, evaluated starting from its hardness on Shore A scale σ_A, according to conversion function presented in [34]:

$$log_{10}(E) = 0.0235\sigma_A - 0.6403.$$

In accordance with eq. (8), the theoretical maximum forces is function of the end-effector orientation angles (Fig. 4a) that can be evaluated starting from pin position:

$$\alpha = \arctan\left(\frac{r_z}{r_y}\right), \text{ and } \beta = \arctan\left(\frac{r_z}{r_x}\right).$$

IV. Force Evaluation

On other hand several tests on four discrete points on pad were carried out to evaluate the real HAPP maximum forces. The tests investigated force on four discretized points, reported in Tab. II and shown in Fig 4b, inside a quarter of pad circumference, the results are extendable to complete pad for central symmetry of its geometry. The tests consisted of N end-effector indentation repetitions to apply the maximum forces on the hand of a user, with $N = 10$. The force values are collected by a high-precision ATI force sensor (ATI Industrial Automation Inc., US), placed between pad and human hand by means of glove pocket. Only one subject was involved into force testing, he gave his written informed consent to participate, and was able to discontinue participation at any time during experiments. The experiment protocols followed the declaration of Helsinki, and there was no risk of harmful effects on subjects' health. Data were

Fig. 6: From left to right, the nine discrete positions reached by the haptic device.

TABLE III: ID signals and their values sent from graphic user interface to microcontroller for HAPP setting, regulation, actuation, and control.

Reference signal	ID	Values
Stimualtion type	s	$[s, v]$
Anthropometric dimensions	d	$[L, M, S]$
Stimulation 1	v	$[0 - 255]$
Stimulation 2	f	$[0 - 255]$
Desired position	p	$[1 - 9]$

acquired at frequency of 1kHz. Each pressure peaks were maintained and suspended for a time equal to $\delta t = 8.0$s. The recorded forces $\tilde{\boldsymbol{f}}(t)$ are analysed to extrapolate information about the net forces applied by HAPP, $\tilde{\boldsymbol{f}}_n$, as:

$$\tilde{\mathbf{f}}_n = \frac{1}{2N\delta t} \sum_{n=0}^{N} \left| \sum_{t=n\delta t}^{(n+1)\delta t} \tilde{\mathbf{f}}(t) - \sum_{t=(n+1)\delta t}^{(n+2)\delta t} \tilde{\mathbf{f}}(t) \right|.$$

To reconstruct the force distribution pad surface was conducted a interpolation on collected data, between several mathematical interpolating 3D functions we choose a Thin-plane spline model with a goodness of fit equal to $R^2 = 0.97$. The experimental results, graphically reported in Fig. 4b shown a general reduced maximum forces respect the theoretical estimation, in addition the tests shown that the user over 10 N started to detach the hand from the pad.

V. Demonstrative scenario

HAPP was designed so that researchers and doctors can set up and control the device by using their laptop, in particular they can choose the desired position, force and other stimulus references as well as initial information about the discrete anthropometric dimensions that are then sent to the device via USB cable. For this purpose, the operator has a graphical user interface (GUI) that allows the easy setting of the stimuli through percentage bars and the placement of the piston in one of the nine discrete areas on the patient's palm (See Fig. 5). The graphical interface is easily expandable and is extremely modular, allowing the user to modify and increase the contact areas on the request of the researcher and integrate future end-effector modules for further kind of stimulation. The serial connection between laptop and device allows the exchange of data forward and potentially backward allowing the user to view the data provided by the device, such as the force measured by the force sensor, and record them for a retrospective investigation. The communication protocol is optimized to ensure good responsiveness, the references are transmitted forward only if these are modified by the user, the data sent is composed

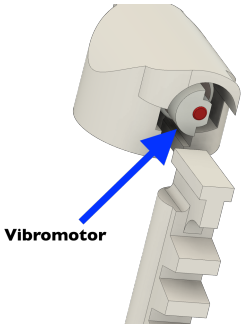

Fig. 7: CAD model for the vibromotor housing.

of two bytes, the first carries a modified reference ID and the second carries the value within a range as reported in Tab. III. Fig. 6 shows the positions that HAPP can reach by using the before presented GUI.

VI. Conclusion

In this paper we presented HAPP, a haptic device for preclinical investigation of the mechanical therapy effects for pathologies/diseases of the hand, such as the complex regional pain syndrome type-I and stroke, and also for the systematic and remote control of the manual therapy exercises by exploiting its graphical user interface. In particular, with this work, we introduced the concept, detailed the mechanical design, and the mathematical model used, with preliminary studies, in order to evaluate the device force exerted at the user's palm. The device uses a parallel 3-DoF structure position and orient its end-effector under the patient's hand palm and provide local force stimulation. HAPP's end-effector is interchangeable and in this work, a solution to exert the desired force in predefined areas of the user's palm was presented. Despite HAPP is in prototyping phase, it received positive opinions from experts of the rehabilitation field, which consider HAPP a promising device for mechanical therapy of the hand. Future works of this study will investigate the integration and control of the vibration stimulus on defined areas of the hand. Also, instead of controlling the device in position, we plan to implement a PID controller. The CAD model of a proof of concept was designed (Fig. 7). Its design is a trade-off between compactness, functionality, portability and capability of satisfying the initial requirements. The graphical user interface was arranged in advance with a bar that allows to set the vibration intensity. Other future works will include structural analysis, design optimization and studies on a control law that takes into account the force, vibration and additional stimulation to be transmitted to the user's palm. Moreover, a detailed

comparison with other devices present in the literature will be done and integration with virtual reality environment systems for gaming, clinical propose, and human studies on device usability will be investigated.

REFERENCES

[1] T. J. Coderre, D. N. Xanthos, L. Francis, and G. J. Bennett, "Chronic post-ischemia pain (cpip): a novel animal model of complex regional pain syndrome-type i (crps-i; reflex sympathetic dystrophy) produced by prolonged hindpaw ischemia and reperfusion in the rat," *Pain*, vol. 112, no. 1-2, pp. 94–105, 2004.

[2] F. Birklein and M. Schmelz, "Neuropeptides, neurogenic inflammation and complex regional pain syndrome (crps)," *Neuroscience letters*, vol. 437, no. 3, pp. 199–202, 2008.

[3] W. S. Kingery, "Role of neuropeptide, cytokine, and growth factor signaling in complex regional pain syndrome," *Pain medicine*, vol. 11, no. 8, pp. 1239–1250, 2010.

[4] C. Maihöfner, F. Seifert, and K. Markovic, "Complex regional pain syndromes: new pathophysiological concepts and therapies," *European Journal of Neurology*, vol. 17, no. 5, pp. 649–660, 2010.

[5] H. M. Oerlemans, R. J. A. Goris, T. De Boo, and R. A. Oostendorp, "Do physical therapy and occupational therapy reduce the impairment percentage in reflex sympathetic dystrophy? 1," *American journal of physical medicine rehabilitation*, vol. 78, no. 6, pp. 533–539, 1999.

[6] T. O. Smith, "How effective is physiotherapy in the treatment of complex regional pain syndrome type 1? a review of the literature," *Musculoskeletal Care*, vol. 3, no. 4, pp. 181–200, 2005.

[7] H. van de Meent, M. Oerlemans, A. Bruggeman, F. Klomp, R. van Dongen, R. Oostendorp, and J. P. Frölke, "Safety of "pain exposure" physical therapy in patients with complex regional pain syndrome type 1," *Pain*, vol. 152, no. 6, pp. 1431–1438, 2011.

[8] P. Moss, K. Sluka, and A. Wright, "The initial effects of knee joint mobilization on osteoarthritic hyperalgesia," *Manual therapy*, vol. 12, no. 2, pp. 109–118, 2007.

[9] J. E. Bialosky, M. D. Bishop, D. D. Price, M. E. Robinson, and S. Z. George, "The mechanisms of manual therapy in the treatment of musculoskeletal pain: a comprehensive model," *Manual therapy*, vol. 14, no. 5, pp. 531–538, 2009.

[10] J. Camarinos and L. Marinko, "Effectiveness of manual physical therapy for painful shoulder conditions: a systematic review," *Journal of Manual & Manipulative Therapy*, vol. 17, no. 4, pp. 206–215, 2009.

[11] D. F. Martins, F. Bobinski, L. Mazzardo-Martins, F. J. Cidral-Filho, F. P. Nascimento, V. M. Gadotti, and A. R. Santos, "Ankle joint mobilization decreases hypersensitivity by activation of peripheral opioid receptors in a mouse model of postoperative pain," *Pain Medicine*, vol. 13, no. 8, pp. 1049–1058, 2012.

[12] D. Martins, L. Mazzardo-Martins, F. Cidral-Filho, V. Gadotti, and A. Santos, "Peripheral and spinal activation of cannabinoid receptors by joint mobilization alleviates postoperative pain in mice," *Neuroscience*, vol. 255, pp. 110–121, 2013.

[13] A. S. Salgado, J. Stramosk, D. D. Ludtke, A. C. Kuci, D. C. Salm, L. A. Ceci, F. Petronilho, D. Florentino, L. G. Danielski, A. Gassenferth, *et al.*, "Manual therapy reduces pain behavior and oxidative stress in a murine model of complex regional pain syndrome type i," *Brain sciences*, vol. 9, no. 8, p. 197, 2019.

[14] A. J. Beaudoin, F. Pedneault, M. Houle, C. Bilodeau, M.-P. Gauvin, D. Groleau, P. Brochu, and M. Couture, "Case study assessing the feasibility of using a wearable haptic device or humanoid robot to facilitate transitions in occupational therapy sessions for children with autism spectrum disorder," *Journal of Rehabilitation and Assistive Technologies Engineering*, vol. 8, p. 20556683211049041, 2021.

[15] F. Barbic, M. Galli, L. Dalla Vecchia, M. Canesi, V. Cimolin, A. Porta, V. Bari, G. Cerri, F. Dipaola, T. Bassani, *et al.*, "Effects of mechanical stimulation of the feet on gait and cardiovascular autonomic control in parkinson's disease," *Journal of Applied Physiology*, vol. 116, no. 5, pp. 495–503, 2014.

[16] M.-A. Choukou, S. Mbabaali, J. Bani Hani, and C. Cooke, "Haptic-enabled hand rehabilitation in stroke patients: a scoping review," *Applied Sciences*, vol. 11, no. 8, p. 3712, 2021.

[17] H.-C. Wu, Y.-C. Liao, Y.-H. Cheng, P.-C. Shih, C.-M. Tsai, and C.-Y. Lin, "The potential effect of a vibrotactile glove rehabilitation system on motor recovery in chronic post-stroke hemiparesis," *Technology and Health Care*, vol. 25, no. 6, pp. 1183–1187, 2017.

[18] E. B. Brokaw, T. M. Murray, T. Nef, P. S. Lum, D. Nichols, and R. J. Holley, "Time independent functional task training: a case study on the effect of inter-joint coordination driven haptic guidance in stroke therapy," in *2011 IEEE International Conference on Rehabilitation Robotics*, pp. 1–6, IEEE, 2011.

[19] A. A. Timmermans, R. J. Lemmens, M. Monfrance, R. P. Geers, W. Bakx, R. J. Smeets, and H. A. Seelen, "Effects of task-oriented robot training on arm function, activity, and quality of life in chronic stroke patients: a randomized controlled trial," *Journal of neuroengineering and rehabilitation*, vol. 11, no. 1, pp. 1–12, 2014.

[20] G. G. Fluet, A. S. Merians, Q. Qiu, A. Davidow, and S. V. Adamovich, "Comparing integrated training of the hand and arm with isolated training of the same effectors in persons with stroke using haptically rendered virtual environments, a randomized clinical trial," *Journal of neuroengineering and rehabilitation*, vol. 11, no. 1, pp. 1–11, 2014.

[21] R. C. Loureiro, W. S. Harwin, R. Lamperd, and C. Collin, "Evaluation of reach and grasp robot-assisted therapy suggests similar functional recovery patterns on proximal and distal arm segments in sub-acute hemiplegia," *IEEE Transactions on Neural Systems and Rehabilitation Engineering*, vol. 22, no. 3, pp. 593–602, 2013.

[22] A. Maris, K. Coninx, H. Seelen, V. Truyens, T. De Weyer, R. Geers, M. Lemmens, J. Coolen, S. Stupar, I. Lamers, *et al.*, "The impact of robot-mediated adaptive i-travle training on impaired upper limb function in chronic stroke and multiple sclerosis," *Disability and Rehabilitation: Assistive Technology*, vol. 13, no. 1, pp. 1–9, 2018.

[23] J. Broeren, M. Rydmark, A. Björkdahl, and K. S. Sunnerhagen, "Assessment and training in a 3-dimensional virtual environment with haptics: a report on 5 cases of motor rehabilitation in the chronic stage after stroke," *Neurorehabilitation and neural repair*, vol. 21, no. 2, pp. 180–189, 2007.

[24] X. Huang, F. Naghdy, G. Naghdy, and H. Du, "Clinical effectiveness of combined virtual reality and robot assisted fine hand motion rehabilitation in subacute stroke patients," in *2017 International Conference on Rehabilitation Robotics (ICORR)*, pp. 511–515, IEEE, 2017.

[25] M. Bouri, C. Baur, R. Clavel, C. Newman, and M. Zedka, "Handreha": a new hand and wrist haptic device for hemiplegic children," in *ACHI 2013, The Sixth International Conference on Advances in Computer-Human Interactions*, pp. 286–292, 2013.

[26] N. Pernalete, S. Edwards, R. Gottipati, J. Tipple, V. Kolipakam, and R. V. Dubey, "Eye-hand coordination assessment/therapy using a robotic haptic device," in *9th International Conference on Rehabilitation Robotics, 2005. ICORR 2005.*, pp. 25–28, IEEE, 2005.

[27] N. Pernalete, R. Gottipati, J. Grantner, S. Edwards, D. Janiak, J. Haskin, and R. Dubey, "Integration of an intelligent decision support system and a robotic haptic device for eye-hand coordination therapy," in *2007 IEEE 10th International Conference on Rehabilitation Robotics*, pp. 283–291, IEEE, 2007.

[28] M. Ferre, I. Galiana, R. Wirz, and N. Tuttle, "Haptic device for capturing and simulating hand manipulation rehabilitation," *IEEE/ASME Transactions on Mechatronics*, vol. 16, no. 5, pp. 808–815, 2011.

[29] M. Dragusanu, A. Villani, D. Prattichizzo, and M. Malvezzi, "Design of a wearable haptic device for hand palm cutaneous feedback," *Frontiers in Robotics and AI*, p. 254, 2021.

[30] C. Pacchierotti, G. Salvietti, I. Hussain, L. Meli, and D. Prattichizzo, "The hring: A wearable haptic device to avoid occlusions in hand tracking," in *2016 IEEE Haptics Symposium (HAPTICS)*, pp. 134–139, IEEE, 2016.

[31] M. Malvezzi, T. L. Baldi, A. Villani, F. Ciccarese, and D. Prattichizzo, "Design, development, and preliminary evaluation of a highly wearable exoskeleton," in *2020 29th IEEE International Conference on Robot and Human Interactive Communication (RO-MAN)*, pp. 1055–1062, IEEE, 2020.

[32] M. Dragusanu, D. Troisi, A. Villani, D. Prattichizzo, and M. Malvezzi, "Design and prototyping of an underactuated hand exoskeleton with fingers coupled by a gear-based differential," *Frontiers in Robotics and AI*, p. 69.

[33] M. Dragusanu, T. L. Baldi, Z. Iqbal, D. Prattichizzo, and M. Malvezzi, "Design, development, and control of a tendon-actuated exoskeleton for wrist rehabilitation and training," in *2020 IEEE International Conference on Robotics and Automation (ICRA)*, pp. 1749–1754, IEEE, 2020.

[34] K. Larson, "Can you estimate modulus from durometer hardness for silicones," *Dow Corning Corporation*, pp. 1–6, 2016.